

Searching for Nearby Diffuse Dwarf Galaxies in the COSMOS Field

DongDong Shi^{1,*}, XianZhong Zheng^{2,*}, Zhizheng Pan³, Yu Luo⁴, Hongxia Deng¹, Qunzhi Hua¹, Xinyu Luo¹ and Qiming Wu¹

¹Center for Fundamental Physics, School of Mechanics and Optoelectronic Physics, Anhui University of Science and Technology, Huainan 232001, China

²Tsung-Dao Lee Institute and Key Laboratory for Particle Physics, Astrophysics and Cosmology, Ministry of Education, Shanghai Jiao Tong University, Shanghai, 201210, China

³Purple Mountain Observatory, Chinese Academy of Sciences, 10 Yuan Hua Road, Nanjing, Jiangsu 210023, China

⁴Department of Physics, School of Physics and Electronics, Hunan Normal University, Changsha 410081, China

Correspondence*:

DongDong Shi, XianZhong Zheng
ddshi@aust.edu.cn, xzzheng@sjtu.edu.cn

ABSTRACT

It remains challenging to systematically survey nearby diffuse dwarf galaxies and address the formation mechanism of this population distinguishing from regular ones. We carry out a pilot search for these galaxies in the COSMOS field using the deep *HST*/F814W imaging data. We report three diffuse dwarf galaxies satisfying the criteria: (1) redshift $z < 0.2$, (2) effective radius $r_e > 1''.0$, and (3) central surface brightness $\mu_0 > 24 \text{ mag arcsec}^{-2}$. Two of the three galaxies, COSMOS-UDG1 and COSMOS-UDG2, are recognized as ultra-diffuse galaxies (UDGs) with redshift $z = 0.130$ and 0.049 , respectively. The third galaxy, COSMOS-dw1, is spectroscopically confirmed as a dwarf galaxy at $z = 0.004$. We derive the physical properties through fitting their spectral energy distributions (SEDs) extracted from deep multiwavelength observations. COSMOS-dw1 has a stellar mass of $5.6_{-2.7}^{+2.5} \times 10^6 M_\odot$, harboring neutral hydrogen gas of mass $4.90 \pm 0.90 \times 10^6 M_\odot$, hinting that this galaxy may be in the nascent stages of quenching. The estimated dynamical mass of $3.4 \times 10^7 M_\odot$ further suggests that COSMOS-dw1 is predominantly of dark matter. COSMOS-UDG1 and COSMOS-UDG2 exhibit comparable stellar masses of $\sim 2 \times 10^8 M_\odot$. Notably, COSMOS-UDG1 is younger and more metal-rich than COSMOS-UDG2 and COSMOS-dw1. Conversely, COSMOS-UDG2 and COSMOS-dw1 have similar stellar metallicities, yet COSMOS-UDG2 is older than COSMOS-dw1. All three galaxies adhere to the stellar mass-metallicity relation (MZR) for dwarf galaxies in the local Universe, implying they belong to the dwarf galaxy population.

Keywords: Galaxy formation; Galaxy evolution; COSMOS field; Ultra-diffuse galaxies; Dwarf galaxies; Extragalactic astronomy

1 INTRODUCTION

The extremely low surface brightness (LSB) galaxies in the Universe provide crucial insights into galaxy formation and evolution, particularly concerning the role of dark matter and the mechanisms shaping diverse galaxy morphologies (e.g., Impey & Bothun, 1997; Bullock & Boylan-Kolchin, 2017). Ultra-diffuse galaxies (UDGs) are distinguished by their extremely low central surface brightness $\mu(g, 0) > 24 \text{ mag arcsec}^{-2}$, large half-light radius ($r_e > 1.5 \text{ kpc}$) comparable to that of typical L^* galaxies and relatively low stellar mass ($<\sim 10^8 M_\odot$), which is two orders of magnitude smaller than that of L^* galaxies (van Dokkum et al., 2015a). It remains unclear whether these extreme properties arise from distinct formation processes compared to normal galaxies.

UDGs have been found in a variety of environments, including galaxy clusters (e.g., van Dokkum et al., 2015a; Koda et al., 2015; Mihos et al., 2015; Muñoz et al., 2015; Martínez-Delgado et al., 2016; van der Burg et al., 2016; Román & Trujillo, 2017a; Janssens et al., 2017; Lee et al., 2017, 2020; Iodice et al., 2020; Wittmann et al., 2017; Janssens et al., 2019; Gannon et al., 2022; Venhola et al., 2022; La Marca et al., 2022a,b), groups (e.g., Smith Castelli et al., 2016; Merritt et al., 2016; Ordenes-Briceño et al., 2016; Trujillo et al., 2017; Román & Trujillo, 2017b; Shi et al., 2017; van der Burg et al., 2017; Müller et al., 2018; Greco et al., 2018a; Somalwar et al., 2020; Zaritsky et al., 2023; Jones et al., 2023) and the fields (e.g., Bellazzini et al., 2017; Leisman et al., 2017; Bennet et al., 2018; Prole et al., 2019; Barbosa et al., 2020; Fielder et al., 2024; Montes et al., 2024), as well as within cosmic void (Román et al., 2019) and associated with the large-scale structures (e.g., Román & Trujillo, 2017a; Shi et al., 2017). Accumulating observational evidence reveals that UDGs exhibit a diverse range of properties. They can be red and blue in color (e.g., Koda et al., 2015; Román & Trujillo, 2017a,b; Shi et al., 2017; Leisman et al., 2017), gas-poor and gas-rich in H I gas content (e.g., Trujillo et al., 2017; Kadovski et al., 2017; Bellazzini et al., 2017; Papastergis et al., 2017; Spekkens & Karunakaran, 2018; Karunakaran et al., 2020, 2024), and have prolate and oblate in geometry/intrinsic ellipticity distribution (Burkert, 2017). Some UDGs contain a high fraction of globular clusters (GCs) (e.g., Beasley et al., 2016; Beasley & Trujillo, 2016; Peng & Lim, 2016; van Dokkum et al., 2016, 2017, 2018a; Toloba et al., 2018; Lim et al., 2018; Marleau et al., 2024; Forbes et al., 2025), and many host a compact nucleus in their central regions (e.g., Yagi et al., 2016; Janssens et al., 2017; Lambert et al., 2024; Khim et al., 2024). These observations suggest that the UDG population, selected based on observational criteria, may be composed of different populations formed through different pathways. For instance, UDGs Dragonfly 44 and Dragonfly X1 are likely overwhelmingly dominated by dark matter and are considered as “failed” galaxies with massive halo ($> 5 \times 10^{11} M_\odot$) (van Dokkum et al., 2015a, 2016, 2017), and UDGs VCC 1287 and Dragonfly 17 are seen as “failed” Large Magellanic Cloud (LMC) or M33 with low halo mass ($< 10^{11} M_\odot$) (Beasley & Trujillo, 2016; Peng & Lim, 2016; Amorisco et al., 2018). In contrast, several UDGs have been reported to be tidally disrupted dwarf galaxies, also known as tidal debris or disturbed UDGs (Mihos et al., 2015, 2017; Merritt et al., 2016; Greco et al., 2018b; Fielder et al., 2024). These typically exhibit lower dark matter halos compared to what is expected for their stellar mass (van Dokkum et al., 2018b; Toloba et al., 2018; Ogiya, 2018). The UDGs, NGC1052-DF2 and DF4, contain little or no dark matter (van Dokkum et al., 2018b,a, 2019; Shen et al., 2021; van Dokkum et al., 2022), although the controversy still remains (Trujillo et al., 2019; Montes et al., 2020).

Multiple formation scenarios have been proposed to account for the extended nature of UDGs. Galaxy collisions in dense environments are suggested as a mechanism for forming UDGs (Baushev, 2018), often leading to prolate rather than oblate morphologies (Burkert, 2017). Carleton et al. (2019) proposed that tidal stripping and heating are primary drivers of UDG formation in the dense environments. In less-dense environments, such as poor clusters and galaxy groups, the interaction of the interstellar medium (ISM)

with the intra-cluster medium (ICM) is believed to play a pivotal role in shaping UDGs (Levy et al., 2007). On the other hand, Amorisco & Loeb (2016) contended that UDGs are predominantly dwarf galaxies with extremely high spins. Leisman et al. (2017) and Spekkens & Karunakaran (2018) reported that gas-rich UDGs tend to reside in halos of high angular momentum traced by H I line width, supporting the high-spin scenario (Amorisco & Loeb, 2016; Rong et al., 2017). Furthermore, gas outflow driven by strong feedback from supernovae and massive star winds in a star-forming galaxy is suggested to cause the expansion of dark matter and stellar disk, ultimately reshaping the galaxy into a faint and extended form (Di Cintio et al., 2017; Chan et al., 2018). In addition, Sales et al. (2020) suggested that UDG population is a mixture of normal LSB galaxies typically found in the low-density environments, along with a distinct population whose expansive size and LSB are a result of the impact of cluster tides (e.g., Tremmel et al., 2020).

Table 1. The properties of COSMOS-dw1, COSMOS-UDG1 and COSMOS-UDG2. The parameters listed from top to bottom rows, refer to coordinates, redshift, magnitude in F606W/F814W, color, central surface brightness in F606W/F814W, effective radius in angular and physical size, Sérsic index (n), axis ratio (b/a), stellar mass $\log(M_*/M_\odot)$, SFR ($M_\odot \text{ yr}^{-1}$), stellar age (Gyr), $\log(\tau/\text{Gyr})$, stellar metallicity $\log(Z/Z_\odot)$ and HII mass, respectively. Note that we correct the extinction, K-correction and cosmological dimming effects.

	COSMOS-dw1	COSMOS-UDG1	COSMOS-UDG2
R.A. (J2000.0)	10:00:30.069	10:00:37.859	10:00:23.752
Decl. (J2000.0)	+02:08:59.07	+02:24:31.86	+02:22:05.87
redshift	0.004	0.130	0.049
V_{606} (mag)	19.90 ± 0.03	22.81 ± 0.11	21.68 ± 0.06
I_{814} (mag)	19.79 ± 0.04	22.56 ± 0.13	21.55 ± 0.07
$V_{606}-I_{814}$ (mag)	0.11 ± 0.05	0.25 ± 0.17	0.13 ± 0.09
$\mu(V_{606}, 0)$ (mag arcsec $^{-2}$)	24.37 ± 0.16	24.86 ± 0.11	24.48 ± 0.15
$\mu(I_{814}, 0)$ (mag arcsec $^{-2}$)	24.36 ± 0.19	24.75 ± 0.13	24.31 ± 0.12
$r_{e,I_{814}}$ ('')	3.42 ± 0.07	1.14 ± 0.07	1.77 ± 0.08
$r_{e,I_{814}}$ (kpc)	0.29 ± 0.01	2.64 ± 0.16	1.70 ± 0.08
Sérsic index (n)	0.20 ± 0.02	0.19 ± 0.07	0.59 ± 0.08
axis ratio (b/a)	0.65 ± 0.01	0.81 ± 0.05	0.61 ± 0.08
$\log(M_*/M_\odot)$	$6.75^{+0.19}_{-0.21}$	$8.39^{+0.33}_{-0.61}$	$8.34^{+0.17}_{-0.21}$
SFR ($M_\odot \text{ yr}^{-1}$)	~ 0.001	~ 0.239	~ 0.008
age (Gyr)	$4.10^{+5.24}_{-2.5}$	$1.70^{+4.41}_{-1.43}$	$5.58^{+5.10}_{-3.12}$
$\log(\tau/\text{Gyr})$	$0.23^{+0.60}_{-0.80}$	$0.50^{+0.97}_{-0.85}$	$0.07^{+0.52}_{-0.71}$
$\log(Z/Z_\odot)$	$-1.47^{+0.63}_{-0.39}$	$-0.74^{+0.54}_{-0.86}$	$-1.44^{+0.65}_{-0.40}$
$\log(M_{\text{HI}}/M_\odot)$	6.69 ± 0.08

More observational efforts are eagerly demanded to determine the physical properties of UDGs for a better understanding of their origin. Notably, spectroscopic observations are crucial for revealing the properties of stellar populations, metallicity and kinematics. However, it is very expensive to obtain good-quality spectroscopic data for UDGs even with 10 meter-class telescopes. To date, only ≤ 100 UDGs have been spectroscopically observed, and most of them are cluster UDGs (e.g., van Dokkum et al., 2015b, 2016; Martínez-Delgado et al., 2016; Trujillo et al., 2017; Kadawaki et al., 2017; Gu et al., 2018; Ferré-Mateu et al., 2018; Ruiz-Lara et al., 2018; Buzzo et al., 2022, 2024a; Gannon et al., 2024; Shen et al., 2024). These cluster UDGs are mainly dominated by old and metal-poor populations (Kadawaki et al., 2017; Ferré-Mateu et al., 2018; Ruiz-Lara et al., 2018; Iodice et al., 2023). On the other hand, some UDGs (e.g., DGSAT 1 and UGC 2162) in low-density environments seem to consist of relatively young and high-metallicity stellar populations (Martínez-Delgado et al., 2016; Trujillo et al., 2017; Pandya et al., 2018). Moreover, some blue UDGs appear to be gas-rich galaxies so that the 21 cm line can be used to measure the distance of UDGs

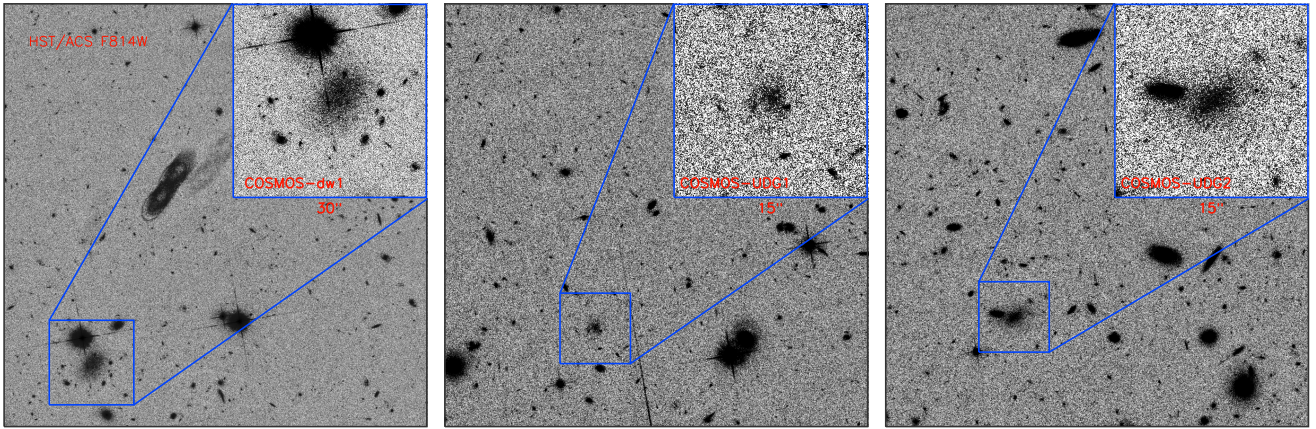


Figure 1. The *HST/ACS* F814W stamps of three COSMOS diffuse galaxies: COSMOS-dw1 (*left*), COSMOS-UDG1 (*middle*), and COSMOS-UDG2 (*right*). The size of the stamps is $90'' \times 90''$. The inner box shows a region of $30'' \times 30''$ for COSMOS-dw1, and $15'' \times 15''$ for COSMOS-UDG1 and COSMOS-UDG2.

and test their formation mechanisms (Trujillo et al., 2017; Papastergis et al., 2017; Bellazzini et al., 2017; Leisman et al., 2017; Shi et al., 2017; Spekkens & Karunakaran, 2018). Additionally, only a few UDGs have been observed for measuring their stellar kinematics through spectroscopy (e.g., Chilingarian et al., 2019; van Dokkum et al., 2019; Iodice et al., 2023), revealing that their dark matter content and velocity profile are diverse (e.g., Emsellem et al., 2019; Kravtsov, 2024). Most UDGs have a large dark matter fraction than dwarf galaxies with similar luminosities, but several UDGs contain little or no dark matter (van Dokkum et al., 2018b,a, 2019; Shen et al., 2021; van Dokkum et al., 2022). Buttitta et al. (2025) mapped the stellar kinematics of some UDGs in the Hydra-I cluster, finding that seven UDGs are in a mild rotation and five UDGs show no evidence of rotation. Recently, some works explored the stellar populations of UDGs using the multiwavelength SED fitting, and concluded that their properties are diverse (e.g., Pandya et al., 2018; Gu et al., 2018; Buzzo et al., 2022, 2024a). Therefore, further investigation of the physical properties of these diffuse galaxies is imperative.

In this work, we systematically search for extremely LSB galaxies in the COSMOS field. The availability of pre-existing deep multiwavelength observations, spanning from the ultraviolet (UV) to the radio, enables us to delve into the properties of these galaxies in detail. In Section 2, we describe the selection of the three diffuse galaxies and the photometric data. Section 3 presents the photometry and analysis. Finally, we discuss and summarize our results in Section 4. We adopt a cosmology with $\Omega_M = 0.3$, $\Omega_\Lambda = 0.7$ and $H_0 = 70 \text{ km s}^{-1} \text{ Mpc}^{-1}$, and the AB magnitude system throughout this work.

2 TARGET SELECTION AND DATA

We carry out a search for UDGs within the central $36' \times 14'$ region of the COSMOS field, where *HST/ACS* F606W (V_{606}) and F814W (I_{814}) observations are available from the 3D-HST/CANDELS survey (van Dokkum et al., 2013; Momcheva et al., 2016). We made use of the 3D-HST redshift and photometric catalog of 33 879 objects (the v4.1.5 release) based on the I_{814} detection to select UDG candidates. We limit redshift at $z < 0.2$, and apply the selection criteria of $\mu(I_{814}, 0) > 24.0 \text{ mag arcsec}^{-2}$ and effective radius $r_e > 1.5 \text{ kpc}$ to the catalog, yielding a sample of ~ 20 objects as the UDG candidates. We visually examine the I_{814} images of these targets to get rid of false sources (e.g., blending and compact sources,

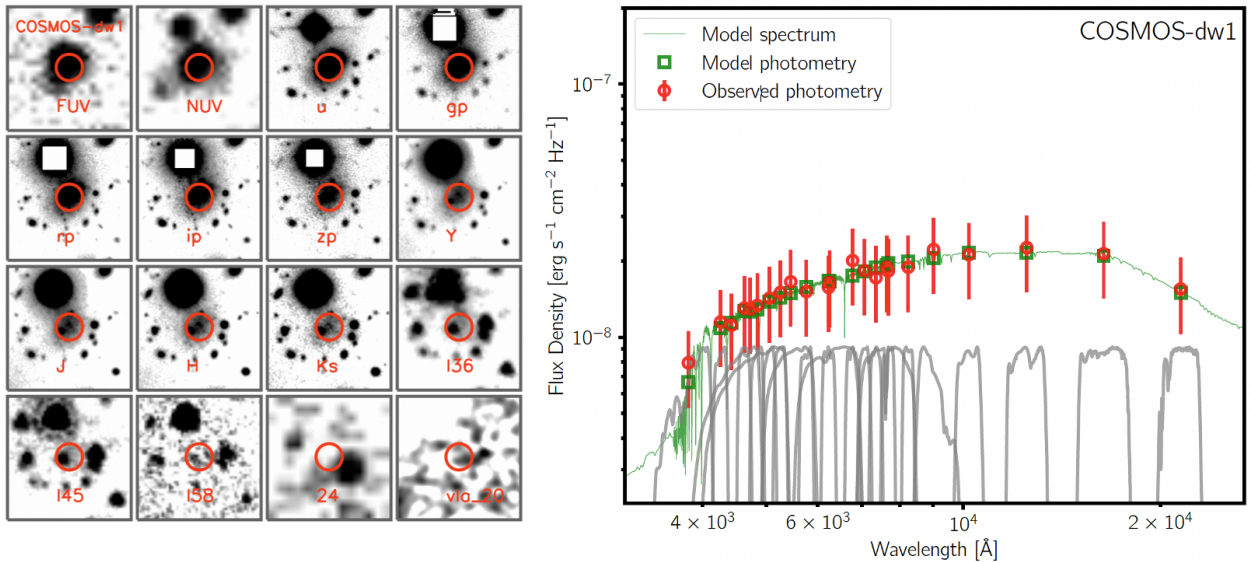


Figure 2. Left: The examples of multiwavelength science images of COSMOS-dw1. The size of each stamp is $30'' \times 30''$. The red circle in each stamp is the target. **Right:** The SED fitting of COSMOS-dw1. The green curve presents the best-fit model from *Prospector*. The grey curves are the filters from optical to NIR. The red points are the observed photometry for COSMOS-dw1, and the green points are the model photometry.

contamination light from the outer of saturate stars). Finally, we obtained three diffuse galaxies, named as COSMOS-dw1, COSMOS-UDG1 and COSMOS-UDG2. Their I_{814} images are shown in Figure 1. Of them, COSMOS-dw1 is not included in the 3D-HST catalog. It was found when visually checked the I_{814} images. We cross correlated these objects with the COSMOS2015 catalog (Laigle et al., 2016), finding that the three objects are all included. We note that COSMOS-dw1 has been confirmed by LRIS on Keck I, and the spectroscopic redshift ($\text{spec-}z$) is 0.0041 (Polzin et al., 2021). The $\text{spec-}z$ of COSMOS-dw1 in radio observations with Five-hundred-meter Aperture Spherical radio Telescope (FAST) and MeerKAT GHz Tiered Extragalactic Explorations (MIGHTEE) HI survey is 0.004 (Pan et al., 2024; Heywood et al., 2024). No $\text{spec-}z$ is available for the rest two objects (although COSMOS-UDG1 was observed through the Very Large Telescope (VLT)/VIMOS spectrograph, there is still no $\text{spec-}z$ due to the low Signal-to-Noise Ratio (SNR) spectrums (Lilly et al., 2007)). The COSMOS2015 catalog provides photo- z of the three objects as 0.005 ± 0.0034 , 0.158 ± 0.008 , 0.044 ± 0.011 , respectively.

The publicly-available multi-band mosaic science images of COSMOS are used to examine the broad properties of the selected UDGs, including Far-UV (FUV) and Near-UV (NUV) images from the Galaxy Evolution Explorer (GALEX) (Zamojski et al., 2007), u and i -band images obtained with Canada-France-Hawaii Telescope (CFHT) (McCracken et al., 2010), Subaru gp , rp , ip , zp and 12 intermediate-band optical images (Taniguchi et al., 2007), deep Y , J , H , and K_s -band images from UltraVISTA (McCracken et al., 2012), IRAC $3.6\ \mu\text{m}$, $4.5\ \mu\text{m}$, $5.8\ \mu\text{m}$, $8\ \mu\text{m}$ data from the COSMOS Spitzer survey (Sanders et al., 2007), and 20 cm data obtained with Very Large Array (VLA) (Schinnerer et al., 2007). More details about these archive data in COSMOS are summarized in Laigle et al. (2016). The left panels of Figure 2, Figure 3 and Figure 4 show the representative multiwavelength images of the three galaxies.

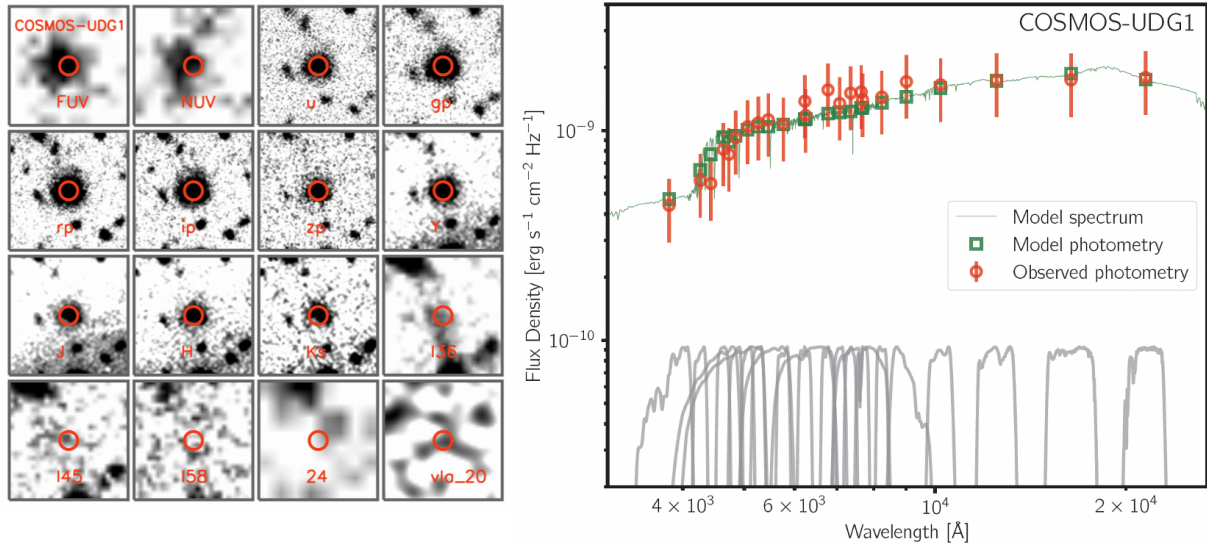


Figure 3. Left: The examples of multiwavelength science images of COSMOS-UDG1. The size of each stamp is $15'' \times 15''$. The red circle in each stamp is the target. **Right:** The SED fitting of COSMOS-UDG1. The green curve presents the best-fit model from *Prospector*. The grey curves are the filters from optical to NIR. The red points are the observed photometry for COSMOS-UDG1, and the green points are the model photometry.

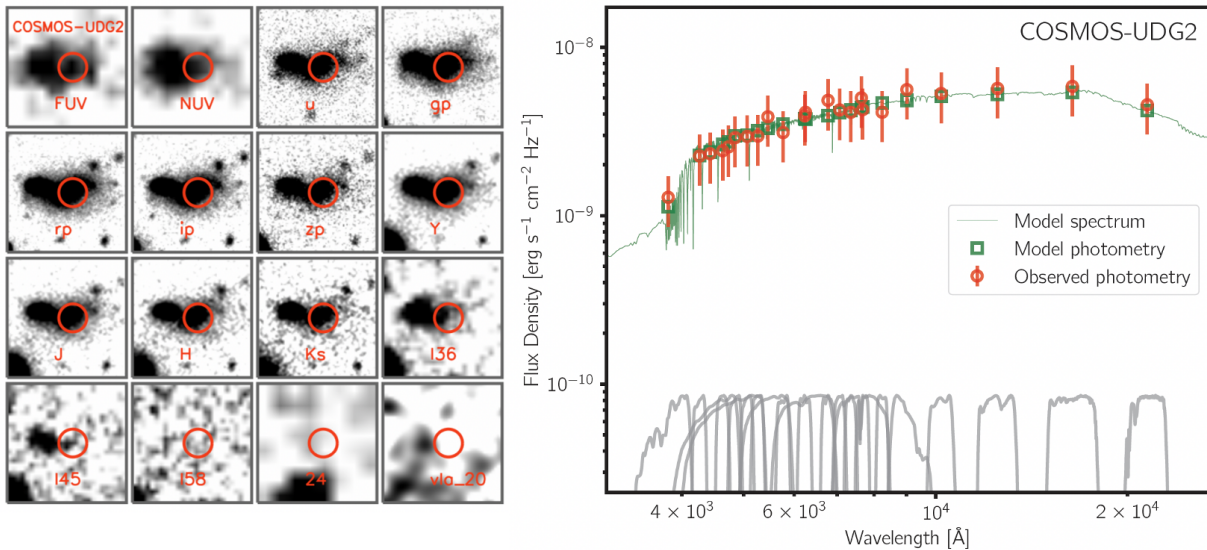


Figure 4. Left: The examples of multiwavelength science images of COSMOS-UDG2. The size of each stamp is $15'' \times 15''$. The red circle in each stamp is the target. **Right:** The SED fitting of COSMOS-UDG2. The green curve presents the best-fit model from *Prospector*. The grey curves are the filters from optical to NIR. The red points are the observed photometry for COSMOS-UDG2, and the green points are the model photometry.

3 PHOTOMETRY AND ANALYSIS

3.1 Aperture-Matched Photometry

We construct aperture-matched SEDs from the FUV to the NIR for our three UDG targets. The three targets are very extended and removal of the blending fluxes from nearby sources is key to measuring

their fluxes. The left panels in Figure 2, Figure 3 and Figure 4 are the examples of mosaics in these three galaxies. Below we describe our processes to derive the aperture-matched photometry from the multi-band imaging data.

For each of our three targets, we cut stamp images of $30'' \times 30''$ centered at the target from mosaic science images for further analysis. We extract the empirical Point Spread Functions (PSF) from the mosaic science images using the software PSF Extractor (PSFEx, version 3.9.1, Bertin, 2011). SExtractor (Bertin & Arnouts, 1996) is used to detect sources and extract their photometric and geometric parameters, including coordinates, magnitude, effective radius r_e , axis ratio (b/a) and position angle (PA). The detection configuration is optimized for individual stamp images. All sources in one stamp image are simultaneously fitted with 2-D Sérsic models using GALFIT (Peng et al., 2002, 2010). The best-fit Sérsic models of detected sources are subtracted from the stamp image and the central target is left. Doing so we obtained clean images of the target. These clean images are used to match PSFs between different bands and derive aperture-matched photometry. The total magnitude in ip is estimated using the growth curve derived from the ip -band clean image.

We notice that the total magnitude in $HST I_{814}$ is systematically lower than that in ip for all three UDGs. The discrepancy still exists even we measure the total magnitude from the I_{814} image degraded from a pixel scale of $0''.03$ to $0''.15$ (the pixel scale of ip). We point out that this discrepancy is caused by the background subtraction in I_{814} data reduction, for which the box size chosen for background estimate is preferentially optimized for faint and compact sources, but too small for extended UDGs. This leads to an oversubtraction of the outskirts of UDGs and therefore the total magnitude to be lower. The magnitude discrepancy is at a level of ~ 0.2 mag and have marginal effects on the estimate of their geometric parameters. We adopt the parameters from the GALFIT best-fit Sérsic models of I_{814} images and list total magnitude of V_{606} , I_{814} , r_e , Sérsic index n , b/a of our three galaxies in Table 1.

The Subaru optical images we used are already PSF-matched. We use a fixed aperture of radius two times the ip -band effective radius $r_{e,ip}$ to derive the aperture-matched fluxes from the clean images in the gp , rp , ip , and zp and other 12 intermediate bands. For other images, we match the images of a given band and the ip -band to the identical spatial resolution, and then derive aperture-matched flux ratio between the two bands. In practice, we convolve one image with the PSF of the other image and vice versa to match two images to the same spatial resolution. This method works well for our targets because they are extended and relatively bright. Aperture photometry on the PSF-matched images with the same circular aperture (i.e., $\text{radius} = 2 \times r_{e,I_{814}}$) gives aperture-matched flux ratio of the two bands. We derived flux ratios of CFHT u and i , UltraVISTA Y , J , H , and K_s to Subaru ip , flux ratios of FUV/NUV to u , and flux ratios of IRAC $3.6\mu\text{m}/4.5\mu\text{m}$ to K_s . These flux ratios based on aperture-matched photometry describe the observed SED over these bands. The observed SED is then normalized to the total magnitude of ip . Taken together, we obtained the FUV-to-NIR SEDs for our three UDG targets, as shown in the right panels of Figure 2 to 4.

We also examine the dust emission of our three galaxies using the deepest $850\mu\text{m}$ map obtained with SCUBA-2 on board James Clerk Maxwell Telescope (JCMT) through the S2COSMOS survey (Casey et al., 2013; Geach et al., 2016; Michałowski et al., 2017), finding no detection at a level of $3\sigma = 1.2\text{ mJy}$. These suggest a very low rate of obscured star formation among our sample objects.

3.2 Modeling of the observed SEDs

Using the software Easy and Accurate Redshifts from Yale (EAZY) (Brammer et al., 2008), we can estimate photometric redshift ($\text{photo-}z$) from the multiwavelength photometric data. The default library of galaxy templates in EAZY is adopted. The input parameters (e.g., templates, input file, output files and

redshift grid) are set in the configuration file. The redshift range we have set is from 0 to 2, incremented by 0.001 each step. Therefore, the photo- z for COSMOS-dw1, COSMOS-UDG1 and COSMOS-UDG2 are 0.010, 0.130 and 0.049, which are fully consistent with the photo- z provided by COSMOS2015 catalog. However, considering that COSMOS-dw1 already has a spectral redshift ($\text{spec-}z = 0.0041$), we use the $\text{spec-}z$ in following SED fitting. The results are listed in Table 1.

We constrain the star formation histories (SFHs) of these three galaxies using the SED fitting technique. The fitting is performed using *Prospector* (Leja et al., 2017, 2019), which uses the Flexible Stellar Population Synthesis (FSPS) package with fully Bayesian Bayesian Markov chain Monte Carlo (MCMC) code (Conroy et al., 2009). We use the default Stellar Population Synthesis (SPS) parameters in FSPS. For the SED modeling, we adopt the Chabrier (2003) IMF and the Calzetti et al. (2000) dust attenuation law. The delayed exponentially declining SFH ($\text{SFR} \sim t \times \exp(-t/\tau)$) is used, where t is time from the formation. The redshift is fixed by $\text{spec-}z$ or photo- z .

The best-fit models of these three galaxies with *Prospector* are shown in the right panels of the Figure 2, Figure 3 and Figure 4. For COSMOS-dw1, we obtain stellar mass $M_* = 5.6_{-2.7}^{+2.5} \times 10^6 M_\odot$, the same as calculated in Polzin et al. (2021). The estimated stellar metallicity, star formation rate (SFR) and stellar age of COSMOS-dw1 is $\log(Z/Z_\odot) = -1.47_{-0.39}^{+0.63}$, $0.001 M_\odot \text{ yr}^{-1}$ and $4.10_{-2.5}^{+5.24} \text{ Gyr}$, respectively. Polzin et al. (2021) claim that COSMOS-dw1 is an isolated quenched low-mass galaxies with strong Balmer absorption lines in the local group, but the specific stellar age and metallicity are not given. Our results support that COSMOS-dw1 has very little star formation at present. For COSMOS-UDG1, we obtain stellar mass $M_* = 2.5_{-3.4}^{+1.9} \times 10^8 M_\odot$, stellar metallicity $\log(Z/Z_\odot) = -0.74_{-0.86}^{+0.54}$, stellar age $1.70_{-1.43}^{+4.41} \text{ Gyr}$. The parameter of stellar mass, stellar metallicity and stellar age in COSMOS-UDG2 is $M_* = 2.2_{-1.1}^{+0.9} \times 10^8 M_\odot$, $\log(Z/Z_\odot) = -1.44_{-0.40}^{+0.65}$ and $5.58_{-3.12}^{+5.10} \text{ Gyr}$, respectively. We find that these three galaxies exhibit diverse properties. COSMOS-UDG1 and COSMOS-UDG2 have similar stellar masses, but COSMOS-UDG1 is younger and more metal-rich than COSMOS-UDG2 and COSMOS-dw1. COSMOS-UDG2 and COSMOS-dw1 have similar stellar metallicities, but COSMOS-UDG2 is older than COSMOS-dw1.

In Figure 5, we show the stellar mass–metallicity relation (MZR) for these three COSMOS galaxies, compared to the relation found for the dwarfs (Kirby et al., 2013) and giant galaxies in the local Universe (Gallazzi et al., 2005). The MZR with large scatter appears to be continuous from low to high masses. Despite the large uncertainties of metallicity and stellar mass, COSMOS-dw1 obeys the MZR at the low mass end, COSMOS-UDG1 and COSMOS-UDG2 follow the MZR defined by normal dwarf galaxies. This suggests that stellar mass plays an important role in determining stellar metallicities, regardless of the size of a galaxy.

4 DISCUSSION AND SUMMARY

We present the physical properties of three nearby diffuse galaxies identified in the central region of the COSMOS field, which is covered by the 3D-HST/CANDELS survey. The primary uncertainty in our analysis is the distances of the three diffuse galaxies. The photometric redshifts derived from the broadband SEDs affirm that these objects are nearby, with redshifts $z < 0.15$. Nevertheless, given uncertainties associated with photo- z , we cannot rule out the possibility that they might be located closer (e.g., in the Local Group), especially for COSMOS-dw1. COSMOS-dw1 has been confirmed by optical spectroscopy

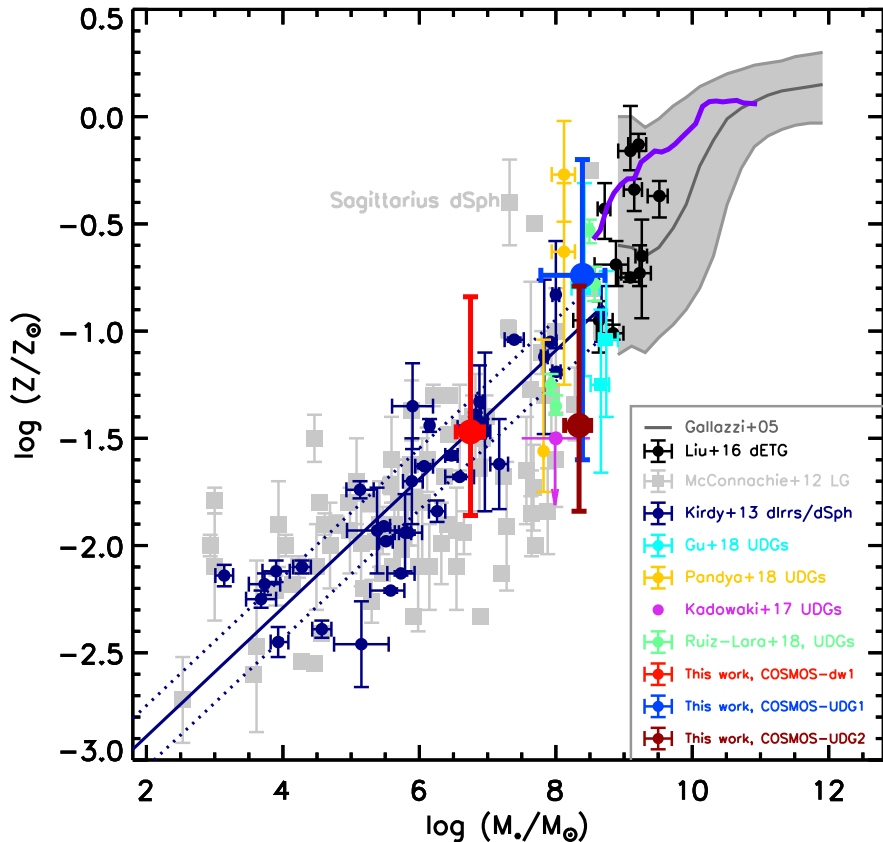


Figure 5. The stellar mass-metallicity relation. The black solid points are the early-type galaxies (ETGs) in Virgo (Liu et al., 2016), dwarf galaxies in and around the Local group are shown in gray solid squares (McConnachie, 2012), and local group dIrrs/dSphs from Kirby et al. (2013) are shown in dark blue solid points, the blue solid line shows the least-squares line, and the dotted lines are the rms about the best fit. MZR relation could extend to the massive galaxies (Gallazzi et al., 2005), as shown the gray solid curves. The purple solid line is the MZR relation of star-forming galaxies with stellar masses ranging between $10^{8.5}$ and 10^{11} M_\odot at $z = 0.027 - 0.25$ (Zahid et al., 2017). Other UDGs from literatures are presented for comparisons (e.g., Kadowaki et al., 2017; Gu et al., 2018; Pandya et al., 2018; Ruiz-Lara et al., 2018). The red, blue and brown solid points stands for the COSMOS-dw1, COSMOS-UDG1 and COSMOS-UDG2, respectively.

and radio observations to have a redshift of 0.004 (Polzin et al., 2021; Pan et al., 2024). For COSMOS-UDG1 and COSMOS-UDG2, we determine their photo-zs to be 0.130 and 0.049, respectively, using multiwavelength data. The physical properties of these three galaxies appear to be strikingly different.

Obtaining accurate distance estimates for the ultra-faint and diffuse objects in local Universe is critical to derive correct galaxy physical properties. Polzin et al. (2021) applied the surface brightness fluctuation (SBF) method to COSMOS-dw1 and measured a distance of $22 \pm 3 \text{ Mpc}$, which aligns with its radial velocity of $1222 \pm 64 \text{ km s}^{-1}$. However, recent work by Foster et al. (2024) used the SBF method to derive distance estimates for the 20 nearby dwarf galaxies detected in the COSMOS field, with COSMOS-dw1 being one of them. The SBF distance is estimated to be $56.3_{-6.7}^{+10.4} \text{ Mpc}$ (Foster et al., 2024), which is three times higher than estimated provided by Polzin et al. (2021). Although Foster et al. (2024) can recover a similar result ($23 \pm 5 \text{ Mpc}$) as Polzin et al. (2021) by modifying certain methodologies, but SBF distance

estimates for the rest galaxies will be severely underestimated ($\sim 10 - 30$ Mpc) after the same modified method is applied to the whole sample. If we adopt the distance of $56.3^{+10.4}_{-6.7}$ Mpc, the estimated stellar mass M_* of COSMOS-dw1 would be an order of magnitude higher than previously estimated, and its effective radius would be three times larger than estimated in the Table 1. Therefore, we emphasize that there are certain discrepancies in the distances derived using the SBF method.

COSMOS-dw1 exhibits a blue color with $V_{606} - I_{814} = 0.11 \pm 0.05$, and has been detected in radio observations to possess HI gas. The HI mass is $M_{\text{HI}} = 4.90 \pm 0.90 \times 10^6 M_\odot$, with the line width W_{50} is 18.2 km s^{-1} , as reported by (Pan et al., 2024). The gas fraction M_{HI}/M_* is 0.87 ± 0.43 , indicating that this galaxy is not gas-poor and still retains a significant amount of atomic gas despite exhibiting quiescent optical spectra (Polzin et al., 2021, top panel of figure 2). Given the isolation, COSMOS-dw1 is unlikely to have undergone strong environmental effects (Polzin et al., 2021). Furthermore, the stellar age of COSMOS-dw1 is estimated to be 4.1 Gyr, suggesting this galaxy formed at $z \sim 0.38$.

The dynamical mass M_{dyn} is estimated using the formula $M_{\text{dyn}} = 3.5 \times 10^5 r_e W_{50}^2 M_\odot$ from Spekkens & Karunakaran (2018), where r_e is effective radius kpc and W_{50} is the line width in units of km s^{-1} . COSMOS-dw1 has $W_{50} = 18.2 \text{ km s}^{-1}$ (Pan et al., 2024). Therefore, we calculate the dynamical mass of COSMOS-dw1 to be $3.36 \pm 0.12 \times 10^7 M_\odot$. Additionally, we estimate the baryonic mass of COSMOS-dw1 as $M_{\text{bar}} = 1.33 M_{\text{HI}} + M_* = 1.21 \pm 0.29 \times 10^7 M_\odot$ (Piña et al., 2019). Assuming the cosmological baryon fraction is 0.16, we derive the virial mass of the dark matter halo to be $7.59 \pm 1.78 \times 10^7 M_\odot$, which is 2 – 3 times higher than the calculated dynamical mass.

The MZR of galaxies offers profound insights into their star formation and chemical enrichment histories. The relatively low scatter in this relation, particularly at the low-mass end (e.g., Kirby et al., 2013), poses a challenge to explain. This relationship is intricately tied to the complex dynamics involving reionization, star formation, gas inflow, outflow, and recycling processes (e.g., Ma et al., 2016).

Recently, numerous researches have unveiled the stellar population properties of some UDGs through optical spectra and multiwavelength photometric data in different environments. These studies have demonstrated the diverse stellar populations of UDGs across different environments. Specifically, UDGs in clusters (e.g., Coma and Virgo) identified by optical spectroscopy are intermediate-to-old age ($> 6 - 10$ Gyr) and metal-poor (e.g., Kadowaki et al., 2017; Ferré-Mateu et al., 2018; Gu et al., 2018; Ruiz-Lara et al., 2018; Villaume et al., 2022; Buzzo et al., 2022; Ferré-Mateu et al., 2023; Gannon et al., 2024; Buzzo et al., 2024a,b). In contrast, some star-forming UDGs in low-density environments are significantly more metal-rich and younger ($\sim < 5$ Gyr) compared to their quiescent counterparts (e.g., Martínez-Delgado et al., 2016; Trujillo et al., 2017; Rong et al., 2020). Using multiwavelength photometric data, several studies have further revealed that UDGs found in clusters are older than those in the field (Pandya et al., 2018; Buzzo et al., 2022). Additionally, some field UDGs showcase stellar populations of intermediate age on average (~ 7 Gyr), with some being metal-poor and others metal-rich (Barbosa et al., 2020).

We examine the environments around the three galaxies, and find that COSMOS-dw1, COSMOS-UDG1 and COSMOS-UDG2 do not have obvious luminous companions, suggesting that all three galaxies reside in the low-density environments. In comparison to UDGs in galaxy clusters (e.g., Kadowaki et al., 2017; Gu et al., 2018; Ruiz-Lara et al., 2018; Buzzo et al., 2022), COSMOS-UDG1 shows younger age and higher metallicity, whereas COSMOS-UDG2 is younger but metal-poor. These observations imply that the relative young ages of COSMOS-UDG1 and COSMOS-UDG2 may be associated with their low-density environment (Martínez-Delgado et al., 2016; Trujillo et al., 2017; Pandya et al., 2018). A possible explanation is that COSMOS-UDG1 have relatively massive halos, more metals can be locked, and finally

reproduce the metal-rich galaxies. Besides, the non-universal initial mass function (IMF) may provide the constraints (Ferré-Mateu et al., 2013). Interestingly, the gray squares in Figure 5 show the Sagittarius (Sgr) dwarf spheroidal (dSph) galaxy, a satellite galaxy in the Milky way, exhibits a relatively high metallicity ($[Fe/H] \sim 0.4$) despite stellar mass is comparable to those of UDGs (Chou et al., 2007; McConnachie, 2012), which is consistent with the results of COSMOS-UDG1.

COSMOS-UDG1 and COSMOS-UDG2 belong to the dwarf galaxies with large size, and their diffuse nature potentially may be governed by internal mechanisms. UDGs are the extended dwarf galaxies with high spin angular momentum (Amorisco & Loeb, 2016; Rong et al., 2017), and strong feedback from supernova or massive stars driven gas outflow, dark matter halo and stellar disks expansion, and reproduce low luminosity and extended galaxies (Di Cintio et al., 2017; Chan et al., 2018). Furthermore, some UDGs may be tidal disturbed dwarf galaxies and some present tidal feature associated with galaxy mergers (Merritt et al., 2016; Greco et al., 2018b). From the deep multiwavelength imaging, the three COSMOS galaxies we identified appear to be no tidal structures. The multiwavelength photometric data can help constrain the properties of these three galaxies, and we look forward to spatially resolving these diffuse galaxies in subsequent work to understand their formation mechanisms.

We summarize our results as follows:

- (1) We conducted a search for a low-mass LSB galaxies (COSMOS-dw1) and two new UDGs (COSMOS-UDG1 and COSMOS-UDG2) within the central region of the COSMOS field, and examine their properties using the existing multiwavelength data. We present their UV-to-IR SEDs built through our careful PSF- and aperture-matched photometry. The spec- z or photo- z in COSMOS-dw1, COSMOS-UDG1 and COSMOS-UDG2 is 0.004, 0.130 and 0.049, respectively.
- (2) SED fitting reveals that these three galaxies exhibit different physical properties. COSMOS-dw1 is a quenched low-mass galaxy with a stellar mass of $5.6_{-2.7}^{+2.5} \times 10^6 M_\odot$. The stellar age and metallicity $\log(Z/Z_\odot)$ of COSMOS-dw1 is $4.10_{-2.5}^{+5.24}$ Gyr and $-1.47_{-0.39}^{+0.63}$, respectively. COSMOS-UDG1 and COSMOS-UDG2 have similar stellar masses ($\sim 10^8 M_\odot$), yet COSMOS-UDG1 is younger and more metal-rich than COSMOS-UDG2 and COSMOS-dw1. COSMOS-UDG2 and COSMOS-dw1 exhibit comparable stellar metallicities, but COSMOS-UDG2 is older than COSMOS-dw1. When compared to cluster UDGs (e.g., Kadowaki et al., 2017; Gu et al., 2018; Ruiz-Lara et al., 2018; Buzzo et al., 2022), COSMOS-UDG1 shows younger age and higher metallicity, whereas COSMOS-UDG2 is younger and metal-poor. This hints that the relatively young ages of COSMOS-UDG1 and COSMOS-UDG2 may be associated with their low-density environment.
- (3) Interestingly, COSMOS-dw1 contains atomic gas with an HI mass of $4.90 \pm 0.90 \times 10^6 M_\odot$, and gas fraction (M_{HI}/M_*) is 0.87 ± 0.43 . This indicates that this galaxy may be in the initial stage of quenching. The estimated dynamical mass is about $3.4 \times 10^7 M_\odot$, implying that COSMOS-dw1 is dominated by dark matter (> 60%).
- (4) Despite the significant uncertainties in metallicity measurements, COSMOS-dw1 aligns with the MZR at the low mass end, while COSMOS-UDG1 and COSMOS-UDG2 broadly follow the MZR established by typical dwarf galaxies. This suggests that stellar mass may be a crucial factor in determining stellar metallicities.

Taken together, the detection of low-luminosity LSB galaxies and UDGs in the COSMOS field indicate that UDGs can indeed be found in random fields. These extreme LSB galaxies identified so far are just the tip of the iceberg. In the future, more unknown LSB galaxies and UDGs could be discovered through multiwavelength imaging facilitated by space- (e.g., Euclid, CSST and Roman) (e.g., Zhan, 2011; Montes

et al., 2023; Euclid Collaboration et al., 2024) and ground-based (e.g., LSST and WFST) telescopes with a wide field-of-view capabilities (e.g., Robertson et al., 2017; Shi et al., 2018; Martin et al., 2022; Breivik et al., 2022; Wang et al., 2023). By combining these observations with spectroscopic analysis, the real natures of UDGs and LSB structures can be fully unveiled.

1 APPENDIX: THE PARAMETER MEASUREMENTS OF THREE UDGs

Here, we have measured the structure parameters of COSMOS-dw1, COSMOS-UDG1 and COSMOS-UDG2 using both 1D Sérsic and 2D Sérsic fitting methods. The structure properties obtained are summarized in Table 2. Figure 6, Figure 7 and Figure 8 depict the 1D surface brightness profiles and 2D Sérsic fitting results for COSMOS-dw1, COSMOS-UDG1 and COSMOS-UDG2, respectively. In the upper panels of Figures 7 and 8, the blue and red points and curves represent the results from the F606W and F814W filters, respectively. The bottom panels of these figures show, from left to right, the original image, the model, and the residual image for each galaxy. The axial ratios (b/a) of these three diffuse galaxies are greater than 0.5, indicating that they exhibit an ellipsoidal shape. Their Sérsic indices $n = 0.53 - 0.91$ suggest that they are similar to typical disk galaxies. From the deep imaging, we find that the three COSMOS galaxies do not exhibit tidal features.

Table 2. The structure properties of COSMOS-dw1, COSMOS-UDG1 and COSMOS-UDG2.

	Sérsic 1D			Sérsic 2D		
	COSMOS-dw1	COSMOS-UDG1	COSMOS-UDG2	COSMOS-dw1	COSMOS-UDG1	COSMOS-UDG2
R.A. (J2000.0)	10:00:30.066	10:00:37.857	10:00:23.792
Decl. (J2000.0)	+02:08:58.880	+02:24:31.990	+02:22:05.660
V_{606} (mag)	19.95	22.94	21.30	19.95	22.94	21.30
I_{814} (mag)	19.72	22.82	21.11	19.72	22.82	21.11
$V_{606} - I_{814}$ (mag)	0.23	0.12	0.19	0.23	0.12	0.19
$\mu(V_{606}, 0)$ (mag arcsec $^{-2}$)	24.38	24.73	24.57	24.33	24.66	24.38
$\mu(I_{814}, 0)$ (mag arcsec $^{-2}$)	24.27	24.33	24.22	24.14	24.35	24.16
$r_{e,I_{814}}$ ('')	3.91	1.03	2.50	3.67	1.22	2.54
Sérsic index (n)	0.55	0.64	0.85	0.53	0.86	0.91
axis ratio (b/a)	0.67	1.0	0.51

CONFLICT OF INTEREST STATEMENT

The authors declare that the research was conducted in the absence of any commercial or financial relationships that could be construed as a potential conflict of interest.

AUTHOR CONTRIBUTIONS

D.D Shi and X.Z Zheng designed the study. D.D Shi led data analyses including the deep multiwavelength imaging, and wrote the original manuscript. Z. Pan and Y. Luo made significant contributions and edits to the text. All authors contributed to the article and approved the submitted version.

FUNDING

This work is supported by Scientific Research Foundation for High-level Talents of Anhui University of Science and Technology (2024yjrc104), the National Science Foundation of China (12303015 and 12173088), and the National Science Foundation of Jiangsu Province (BK20231106).

ACKNOWLEDGMENTS

We thank the referees for the valuable and helpful comments and suggestions, which improve our manuscript. We acknowledge support from Anhui University of Science and Technology and China Manned Space Project.

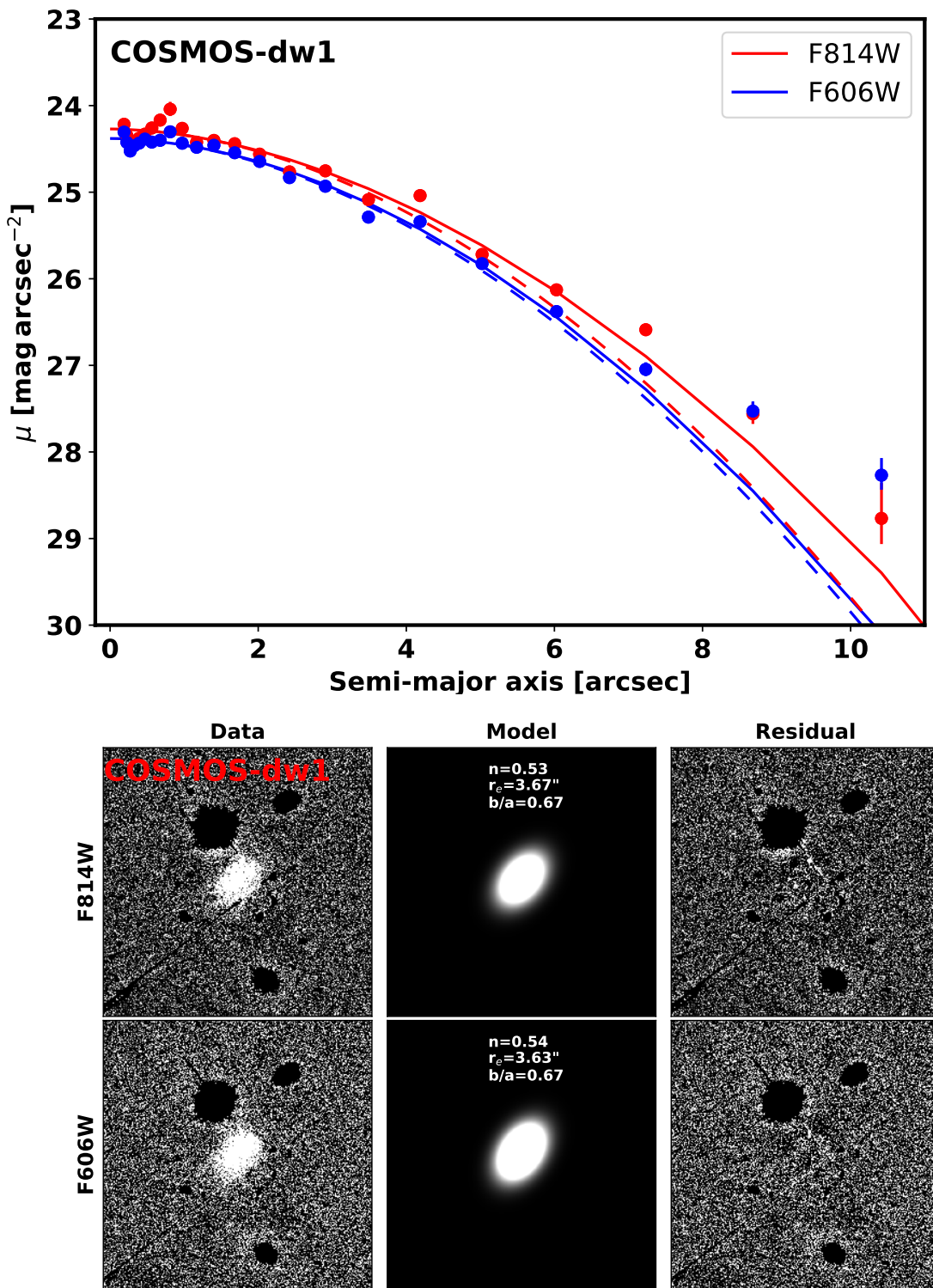


Figure 6. The 1D surface brightness profile (Upper panel) and 2D Sérsic fitting (Bottom panel) of COSMOS-dw1. The size of each stamp is $48'' \times 48''$.

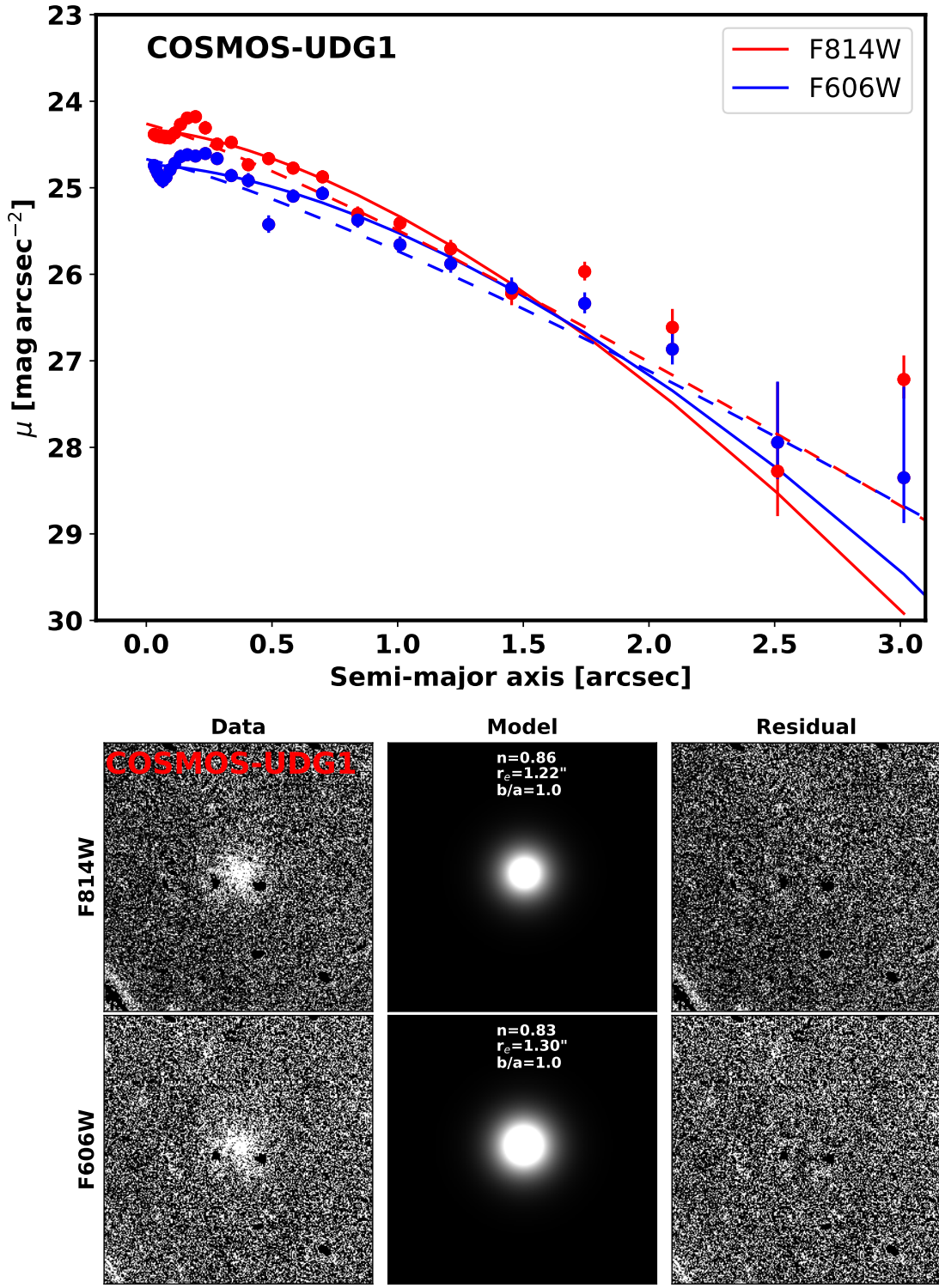


Figure 7. The 1D surface brightness profile (Upper panel) and 2D Sérsic fitting (Bottom panel) of COSMOS-UDG1. The size of each stamp is $15'' \times 15''$.

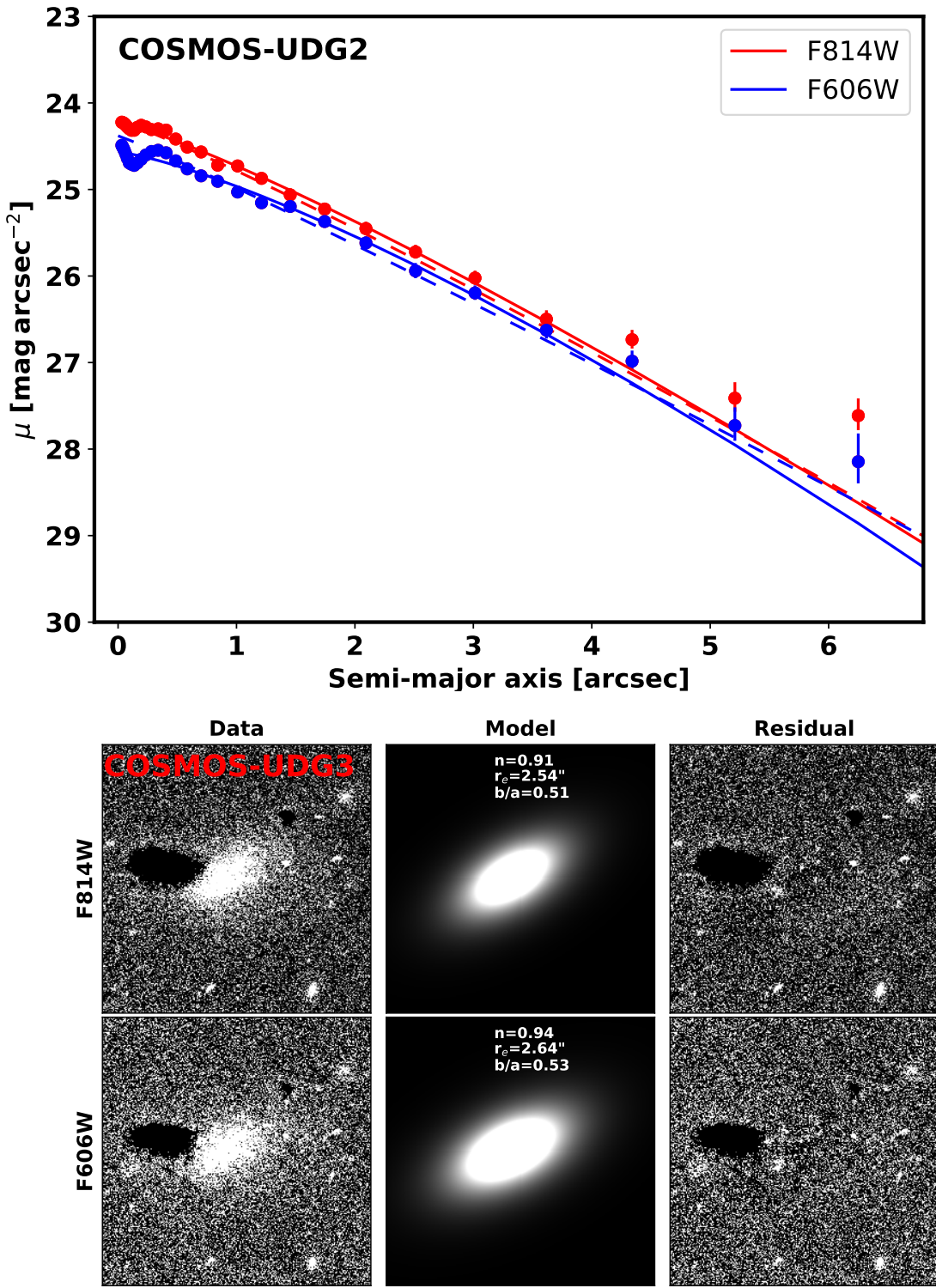


Figure 8. The 1D surface brightness profile (Upper panel) and 2D Sérsic fitting (Bottom panel) of COSMOS-UDG2. The size of each stamp is $15'' \times 15''$.

DATA AVAILABILITY STATEMENT

The raw data supporting the conclusions of this article will be made available by the authors, without undue reservation.

REFERENCES

- Amorisco, N. C., & Loeb, A. 2016, *MNRAS*, 459, L51, doi: 10.1093/mnrasl/slw055
- Amorisco, N. C., Monachesi, A., Agnello, A., & White, S. D. M. 2018, *MNRAS*, 475, 4235, doi: 10.1093/mnras/sty116
- Barbosa, C. E., Zaritsky, D., Donnerstein, R., et al. 2020, *ApJS*, 247, 46, doi: 10.3847/1538-4365/ab7660
- Baushev, A. N. 2018, *Nature*, 60, 69, doi: 10.1016/j.newast.2017.10.008
- Beasley, M. A., Romanowsky, A. J., Pota, V., et al. 2016, *ApJL*, 819, L20, doi: 10.3847/2041-8205/819/2/L20
- Beasley, M. A., & Trujillo, I. 2016, *ApJ*, 830, 23, doi: 10.3847/0004-637X/830/1/23
- Bellazzini, M., Belokurov, V., Magrini, L., et al. 2017, *MNRAS*, 467, 3751, doi: 10.1093/mnras/stx236
- Bennet, P., Sand, D. J., Zaritsky, D., et al. 2018, *ApJL*, 866, L11, doi: 10.3847/2041-8213/aaedf
- Bertin, E. 2011, in Astronomical Society of the Pacific Conference Series, Vol. 442, Astronomical Data Analysis Software and Systems XX, ed. I. N. Evans, A. Accomazzi, D. J. Mink, & A. H. Rots, 435
- Bertin, E., & Arnouts, S. 1996, *A&AS*, 117, 393, doi: 10.1051/aas:1996164
- Brammer, G. B., van Dokkum, P. G., & Coppi, P. 2008, *ApJ*, 686, 1503, doi: 10.1086/591786
- Breivik, K., Connolly, A. J., Ford, K. E. S., et al. 2022, arXiv e-prints, arXiv:2208.02781, doi: 10.48550/arXiv.2208.02781
- Bullock, J. S., & Boylan-Kolchin, M. 2017, *ARA&A*, 55, 343, doi: 10.1146/annurev-astro-091916-055313
- Burkert, A. 2017, *ApJ*, 838, 93, doi: 10.3847/1538-4357/aa671c
- Buttitta, C., Iodice, E., Doll, G., et al. 2025, arXiv e-prints, arXiv:2501.16190, doi: 10.48550/arXiv.2501.16190
- Buzzo, M. L., Forbes, D. A., Brodie, J. P., et al. 2022, *MNRAS*, 517, 2231, doi: 10.1093/mnras/stac2442
- Buzzo, M. L., Forbes, D. A., Jarrett, T. H., et al. 2024a, *MNRAS*, 529, 3210, doi: 10.1093/mnras/stae564
- . 2024b, *MNRAS*, doi: 10.1093/mnras/stae2700
- Calzetti, D., Armus, L., Bohlin, R. C., et al. 2000, *ApJ*, 533, 682, doi: 10.1086/308692
- Carleton, T., Errani, R., Cooper, M., et al. 2019, *MNRAS*, 485, 382, doi: 10.1093/mnras/stz383
- Casey, C. M., Chen, C.-C., Cowie, L. L., et al. 2013, *MNRAS*, 436, 1919, doi: 10.1093/mnras/stt1673
- Chabrier, G. 2003, *Publications of the Astronomical Society of the Pacific*, 115, 763, doi: 10.1086/376392
- Chan, T. K., Kereš, D., Wetzel, A., et al. 2018, *MNRAS*, 478, 906, doi: 10.1093/mnras/sty1153
- Chilingarian, I. V., Afanasiev, A. V., Grishin, K. A., Fabricant, D., & Moran, S. 2019, *ApJ*, 884, 79, doi: 10.3847/1538-4357/ab4205
- Chou, M.-Y., Majewski, S. R., Cunha, K., et al. 2007, *ApJ*, 670, 346, doi: 10.1086/522483
- Conroy, C., Gunn, J. E., & White, M. 2009, *ApJ*, 699, 486, doi: 10.1088/0004-637X/699/1/486

- Di Cintio, A., Brook, C. B., Dutton, A. A., et al. 2017, *MNRAS*, 466, L1, doi: 10.1093/mnrasl/slw210
- Emsellem, E., van der Burg, R. F. J., Fensch, J., et al. 2019, *A&A*, 625, A76, doi: 10.1051/0004-6361/201834909
- Euclid Collaboration, Mellier, Y., Abdurro'uf, et al. 2024, arXiv e-prints, arXiv:2405.13491, doi: 10.48550/arXiv.2405.13491
- Ferré-Mateu, A., Gannon, J. S., Forbes, D. A., et al. 2023, *MNRAS*, 526, 4735, doi: 10.1093/mnras/stad3102
- Ferré-Mateu, A., Vazdekis, A., & de la Rosa, I. G. 2013, *MNRAS*, 431, 440, doi: 10.1093/mnras/stt193
- Ferré-Mateu, A., Alabi, A., Forbes, D. A., et al. 2018, *MNRAS*, 479, 4891, doi: 10.1093/mnras/sty1597
- Fielder, C., Jones, M. G., Sand, D. J., et al. 2024, *AJ*, 168, 212, doi: 10.3847/1538-3881/ad74f6
- Forbes, D. A., Buzzo, M. L., Ferre-Mateu, A., et al. 2025, *MNRAS*, 536, 1217, doi: 10.1093/mnras/stae2675
- Foster, L. M., Taylor, J. E., & Blakeslee, J. P. 2024, *MNRAS*, 527, 1656, doi: 10.1093/mnras/stad3235
- Gallazzi, A., Charlot, S., Brinchmann, J., White, S. D. M., & Tremonti, C. A. 2005, *Monthly Notices of the Royal Astronomical Society*, 362, 41, doi: 10.1111/j.1365-2966.2005.09321.x
- Gannon, J. S., Ferré-Mateu, A., Forbes, D. A., et al. 2024, *Monthly Notices of the Royal Astronomical Society*, 531, 1856, doi: 10.1093/mnras/stae1287
- Gannon, J. S., Forbes, D. A., Romanowsky, A. J., et al. 2022, *MNRAS*, 510, 946, doi: 10.1093/mnras/stab3297
- Geach, J. E., Dunlop, J. S., Halpern, M., et al. 2016, *MNRAS*, 465, 1789, doi: 10.1093/mnras/stw2721
- Greco, J. P., Greene, J. E., Strauss, M. A., et al. 2018a, *ApJ*, 857, 104, doi: 10.3847/1538-4357/aab842
- Greco, J. P., Greene, J. E., Price-Whelan, A. M., et al. 2018b, *PASJ*, 70, S19, doi: 10.1093/pasj/psx051
- Gu, M., Conroy, C., Law, D., et al. 2018, *ApJ*, 859, 37, doi: 10.3847/1538-4357/aabbac
- Heywood, I., Ponomareva, A. A., Maddox, N., et al. 2024, *Monthly Notices of the Royal Astronomical Society*, 534, 76, doi: 10.1093/mnras/stae2081
- Impey, C., & Bothun, G. 1997, *ARA&A*, 35, 267, doi: 10.1146/annurev.astro.35.1.267
- Iodice, E., Cantiello, M., Hilker, M., et al. 2020, *A&A*, 642, A48, doi: 10.1051/0004-6361/202038523
- Iodice, E., Hilker, M., Doll, G., et al. 2023, *A&A*, 679, A69, doi: 10.1051/0004-6361/202347129
- Janssens, S., Abraham, R., Brodie, J., et al. 2017, *ApJL*, 839, L17, doi: 10.3847/2041-8213/aa667d
- Janssens, S. R., Abraham, R., Brodie, J., Forbes, D. A., & Romanowsky, A. J. 2019, *ApJ*, 887, 92, doi: 10.3847/1538-4357/ab536c
- Jones, M. G., Verdes-Montenegro, L., Moldon, J., et al. 2023, *A&A*, 670, A21, doi: 10.1051/0004-6361/202244622
- Kadowaki, J., Zaritsky, D., & Donnerstein, R. L. 2017, *ApJL*, 838, L21, doi: 10.3847/2041-8213/aa653d
- Karunakaran, A., Motiwala, K., Spekkens, K., et al. 2024, *ApJ*, 975, 91, doi: 10.3847/1538-4357/ad77cf

- Karunakaran, A., Spekkens, K., Zaritsky, D., et al. 2020, *ApJ*, 902, 39, doi: 10.3847/1538-4357/abb464
- Khim, D. J., Zaritsky, D., Lambert, M., & Donnerstein, R. 2024, *AJ*, 168, 45, doi: 10.3847/1538-3881/ad4ed3
- Kirby, E. N., Cohen, J. G., Guhathakurta, P., et al. 2013, *ApJ*, 779, 102, doi: 10.1088/0004-637X/779/2/102
- Koda, J., Yagi, M., Yamanoi, H., & Komiyama, Y. 2015, *ApJL*, 807, L2, doi: 10.1088/2041-8205/807/1/L2
- Kravtsov, A. 2024, The Open Journal of Astrophysics, 7, 117, doi: 10.33232/001c.127487
- La Marca, A., Iodice, E., Cantiello, M., et al. 2022a, *A&A*, 665, A105, doi: 10.1051/0004-6361/202142367
- La Marca, A., Peletier, R., Iodice, E., et al. 2022b, *A&A*, 659, A92, doi: 10.1051/0004-6361/202141901
- Laigle, C., McCracken, H. J., Ilbert, O., et al. 2016, *ApJS*, 224, 24, doi: 10.3847/0067-0049/224/2/24
- Lambert, M., Khim, D. J., Zaritsky, D., & Donnerstein, R. 2024, *AJ*, 167, 61, doi: 10.3847/1538-3881/ad0f25
- Lee, J. H., Kang, J., Lee, M. G., & Jang, I. S. 2020, *ApJ*, 894, 75, doi: 10.3847/1538-4357/ab8632
- Lee, M. G., Kang, J., Lee, J. H., & Jang, I. S. 2017, *ApJ*, 844, 157, doi: 10.3847/1538-4357/aa78fb
- Leisman, L., Haynes, M. P., Janowiecki, S., et al. 2017, *ApJ*, 842, 133, doi: 10.3847/1538-4357/aa7575
- Leja, J., Johnson, B. D., Conroy, C., van Dokkum, P. G., & Byler, N. 2017, *ApJ*, 837, 170, doi: 10.3847/1538-4357/aa5ffe
- Leja, J., Johnson, B. D., Conroy, C., et al. 2019, *ApJ*, 877, 140, doi: 10.3847/1538-4357/ab1d5a
- Levy, L., Rose, J. A., van Gorkom, J. H., & Chaboyer, B. 2007, *AJ*, 133, 1104, doi: 10.1086/510723
- Lilly, S. J., Le Fèvre, O., Renzini, A., et al. 2007, *ApJS*, 172, 70, doi: 10.1086/516589
- Lim, S., Peng, E. W., Côté, P., et al. 2018, *ApJ*, 862, 82, doi: 10.3847/1538-4357/aacb81
- Liu, Y., Peng, E. W., Blakeslee, J., et al. 2016, *ApJ*, 818, 179, doi: 10.3847/0004-637X/818/2/179
- Ma, X., Hopkins, P. F., Faucher-Giguère, C.-A., et al. 2016, *MNRAS*, 456, 2140, doi: 10.1093/mnras/stv2659
- Marleau, F. R., Duc, P.-A., Poulain, M., et al. 2024, *A&A*, 690, A339, doi: 10.1051/0004-6361/202449617
- Martin, G., Bazkiae, A. E., Spavone, M., et al. 2022, *MNRAS*, 513, 1459, doi: 10.1093/mnras/stac1003
- Martínez-Delgado, D., Läske, R., Sharina, M., et al. 2016, *AJ*, 151, 96, doi: 10.3847/0004-6256/151/4/96
- McConnachie, A. W. 2012, *AJ*, 144, 4, doi: 10.1088/0004-6256/144/1/4
- McCracken, H. J., Capak, P., Salvato, M., et al. 2010, *ApJ*, 708, 202, doi: 10.1088/0004-637X/708/1/202
- McCracken, H. J., Milvang-Jensen, B., Dunlop, J., et al. 2012, *A&A*, 544, A156, doi: 10.1051/0004-6361/201219507
- Merritt, A., van Dokkum, P., Danieli, S., et al. 2016, *ApJ*, 833, 168, doi: 10.3847/1538-4357/833/2/168
- Michałowski, M. J., Dunlop, J. S., Koprowski, M. P., et al. 2017, *MNRAS*, 469, 492, doi: 10.1093/mnras/stx861

- Mihos, J. C., Harding, P., Feldmeier, J. J., et al. 2017, *ApJ*, 834, 16, doi: 10.3847/1538-4357/834/1/16
- Mihos, J. C., Durrell, P. R., Ferrarese, L., et al. 2015, *ApJL*, 809, L21, doi: 10.1088/2041-8205/809/2/L21
- Momcheva, I. G., Brammer, G. B., van Dokkum, P. G., et al. 2016, *ApJS*, 225, 27, doi: 10.3847/0067-0049/225/2/27
- Montes, M., Infante-Sainz, R., Madrigal-Aguado, A., et al. 2020, *ApJ*, 904, 114, doi: 10.3847/1538-4357/abc340
- Montes, M., Annibali, F., Bellazzini, M., et al. 2023, arXiv e-prints, arXiv:2306.09414, doi: 10.48550/arXiv.2306.09414
- Montes, M., Trujillo, I., Karunakaran, A., et al. 2024, *A&A*, 681, A15, doi: 10.1051/0004-6361/202347667
- Muñoz, R. P., Eigenthaler, P., Puzia, T. H., et al. 2015, *ApJL*, 813, L15, doi: 10.1088/2041-8205/813/1/L15
- Müller, O., Jerjen, H., & Binggeli, B. 2018, *A&A*, 615, A105, doi: 10.1051/0004-6361/201832897
- Ogiya, G. 2018, *MNRAS*, 480, L106, doi: 10.1093/mnrasl/sly138
- Ordenes-Briceño, Y., Taylor, M. A., Puzia, T. H., et al. 2016, *MNRAS*, 463, 1284, doi: 10.1093/mnras/stw2066
- Pan, H., Jarvis, M. J., Zhu, M., et al. 2024, *MNRAS*, 534, 202, doi: 10.1093/mnras/stae2054
- Pandya, V., Romanowsky, A. J., Laine, S., et al. 2018, *ApJ*, 858, 29, doi: 10.3847/1538-4357/aab498
- Papastergis, E., Adams, E. A. K., & Romanowsky, A. J. 2017, *A&A*, 601, L10, doi: 10.1051/0004-6361/201730795
- Peng, C. Y., Ho, L. C., Impey, C. D., & Rix, H.-W. 2002, *AJ*, 124, 266, doi: 10.1086/340952
- . 2010, *AJ*, 139, 2097, doi: 10.1088/0004-6256/139/6/2097
- Peng, E. W., & Lim, S. 2016, *ApJL*, 822, L31, doi: 10.3847/2041-8205/822/2/L31
- Piña, P. E. M., Fraternali, F., Adams, E. A. K., et al. 2019, *The Astrophysical Journal Letters*, 883, L33, doi: 10.3847/2041-8213/ab40c7
- Polzin, A., van Dokkum, P., Danieli, S., Greco, J. P., & Romanowsky, A. J. 2021, *ApJL*, 914, L23, doi: 10.3847/2041-8213/ac024f
- Prole, D. J., van der Burg, R. F. J., Hilker, M., & Davies, J. I. 2019, *MNRAS*, 488, 2143, doi: 10.1093/mnras/stz1843
- Robertson, B. E., Banerji, M., Cooper, M. C., et al. 2017, arXiv e-prints, arXiv:1708.01617, doi: 10.48550/arXiv.1708.01617
- Román, J., Beasley, M. A., Ruiz-Lara, T., & Valls-Gabaud, D. 2019, *MNRAS*, 486, 823, doi: 10.1093/mnras/stz835
- Román, J., & Trujillo, I. 2017a, *MNRAS*, 468, 703, doi: 10.1093/mnras/stx438
- . 2017b, *MNRAS*, 468, 4039, doi: 10.1093/mnras/stx694
- Rong, Y., Guo, Q., Gao, L., et al. 2017, *MNRAS*, 470, 4231, doi: 10.1093/mnras/stx1440
- Rong, Y., Zhu, K., Johnston, E. J., et al. 2020, *ApJL*, 899, L12, doi: 10.3847/2041-8213/aba8aa
- Ruiz-Lara, T., Beasley, M. A., Falcón-Barroso, J., et al. 2018, *MNRAS*, 478, 2034, doi: 10.1093/mnras/sty1112
- Sales, L. V., Navarro, J. F., Peñafiel, L., et al. 2020, *MNRAS*, 494, 1848, doi: 10.1093/mnras/staa854
- Sanders, D. B., Salvato, M., Aussel, H., et al. 2007, *ApJS*, 172, 86, doi: 10.1086/517885

- Schinnerer, E., Smolčić, V., Carilli, C. L., et al. 2007, *ApJS*, 172, 46, doi: 10.1086/516587
- Shen, Z., Danieli, S., van Dokkum, P., et al. 2021, *ApJL*, 914, L12, doi: 10.3847/2041-8213/ac0335
- Shen, Z., Bowman, W. P., van Dokkum, P., et al. 2024, *ApJ*, 976, 75, doi: 10.3847/1538-4357/ad84e2
- Shi, D. D., Zheng, X. Z., Zhao, H. B., et al. 2018, *Acta Astronomica Sinica*, 59, 22
- . 2017, *ApJ*, 846, 26, doi: 10.3847/1538-4357/aa8327
- Smith Castelli, A. V., Faifer, F. R., & Escudero, C. G. 2016, *A&A*, 596, A23, doi: 10.1051/0004-6361/201628969
- Somalwar, J. J., Greene, J. E., Greco, J. P., et al. 2020, *ApJ*, 902, 45, doi: 10.3847/1538-4357/abb1b2
- Spekkens, K., & Karunakaran, A. 2018, *ApJ*, 855, 28, doi: 10.3847/1538-4357/aa94be
- Taniguchi, Y., Scoville, N., Murayama, T., et al. 2007, *ApJS*, 172, 9, doi: 10.1086/516596
- Toloba, E., Lim, S., Peng, E., et al. 2018, *ApJL*, 856, L31, doi: 10.3847/2041-8213/aab603
- Tremmel, M., Wright, A. C., Brooks, A. M., et al. 2020, *MNRAS*, 497, 2786, doi: 10.1093/mnras/staa2015
- Trujillo, I., Roman, J., Filho, M., & Sánchez Almeida, J. 2017, *ApJ*, 836, 191, doi: 10.3847/1538-4357/aa5cbb
- Trujillo, I., Beasley, M. A., Borlaff, A., et al. 2019, *MNRAS*, 486, 1192, doi: 10.1093/mnras/stz771
- van der Burg, R. F. J., Muzzin, A., & Hoekstra, H. 2016, *A&A*, 590, A20, doi: 10.1051/0004-6361/201628222
- van der Burg, R. F. J., Hoekstra, H., Muzzin, A., et al. 2017, *A&A*, 607, A79, doi: 10.1051/0004-6361/201731335
- van Dokkum, P., Brammer, G., Momcheva, I., Skelton, R. E., & Whitaker, K. E. 2013, arXiv e-prints, arXiv:1305.2140, doi: 10.48550/arXiv.1305.2140
- van Dokkum, P., Danieli, S., Abraham, R., Conroy, C., & Romanowsky, A. J. 2019, *ApJL*, 874, L5, doi: 10.3847/2041-8213/ab0d92
- van Dokkum, P., Danieli, S., Cohen, Y., Romanowsky, A. J., & Conroy, C. 2018a, *ApJL*, 864, L18, doi: 10.3847/2041-8213/aada4d
- van Dokkum, P., Abraham, R., Brodie, J., et al. 2016, *ApJL*, 828, L6, doi: 10.3847/2041-8205/828/1/L6
- van Dokkum, P., Abraham, R., Romanowsky, A. J., et al. 2017, *ApJL*, 844, L11, doi: 10.3847/2041-8213/aa7ca2
- van Dokkum, P., Danieli, S., Cohen, Y., et al. 2018b, *Nature*, 555, 629, doi: 10.1038/nature25767
- van Dokkum, P., Shen, Z., Keim, M. A., et al. 2022, *Nature*, 605, 435, doi: 10.1038/s41586-022-04665-6
- van Dokkum, P. G., Abraham, R., Merritt, A., et al. 2015a, *ApJL*, 798, L45, doi: 10.1088/2041-8205/798/2/L45
- van Dokkum, P. G., Romanowsky, A. J., Abraham, R., et al. 2015b, *ApJL*, 804, L26, doi: 10.1088/2041-8205/804/1/L26
- Venhola, A., Peletier, R. F., Salo, H., et al. 2022, *A&A*, 662, A43, doi: 10.1051/0004-6361/202141756
- Villaume, A., Romanowsky, A. J., Brodie, J., et al. 2022, *The Astrophysical Journal*, 924, 32, doi: 10.3847/1538-4357/ac341e
- Wang, T., Liu, G., Cai, Z., et al. 2023, *Science China Physics, Mechanics, and Astronomy*, 66, 109512, doi: 10.1007/s11433-023-2197-5

-
- Wittmann, C., Lisker, T., Ambachew Tilahun, L., et al. 2017, *MNRAS*, 470, 1512, doi: 10.1093/mnras/stx1229
- Yagi, M., Koda, J., Komiyama, Y., & Yamanoi, H. 2016, *ApJS*, 225, 11, doi: 10.3847/0067-0049/225/1/11
- Zahid, H. J., Kudritzki, R.-P., Conroy, C., Andrews, B., & Ho, I. T. 2017, *ApJ*, 847, 18, doi: 10.3847/1538-4357/aa88ae
- Zamojski, M. A., Schiminovich, D., Rich, R. M., et al. 2007, *ApJS*, 172, 468, doi: 10.1086/516593
- Zaritsky, D., Donnerstein, R., Dey, A., et al. 2023, *ApJS*, 267, 27, doi: 10.3847/1538-4365/acdd71
- Zhan, H. 2011, *Scientia Sinica Physica, Mechanica & Astronomica*, 41, 1441, doi: 10.1360/132011-961